ISSN 2176-5480

22nd International Congress of Mechanical Engineering (COBEM 2013)
November 3-7, 2013, Ribeirão Preto, SP, Brazil

DESIGN AND CONSTRUCTION OF A SEMI-ACTIVE FRICTION DAMPER

Freddy A. Murilo Rodriguez
Federal University of Uberlandia
delsius86@hotmail.com

Marcelo Braga dos Santos
Federal University of Uberlandia
mbsantos@mecanica.ufu.br

Francisco Paulo Lepore Neto
Federal University of Uberlandia
fplepore@mecanica.ufu.br

Abstract. *Dry friction dampers have been used for the attenuation of vibrations in mechanical systems such as huge steel structures, turbine blades and other structures where the use of viscous or viscoelastic dampers are forbidden. This paper presents the design of a friction damper which allows the control of the normal force in the contact, resulting in a semi active control system, as the control effort does not act directly on the vibratory system. The objective of this friction damper is maximizing the dissipated vibration energy per cycle of oscillation. This aim could be reached maximizing the energy in each hysteresis cycle. Some techniques to maximize the energy dissipation are presented in this paper, i.e., using numerical simulations these are compared and briefly discussed. Based on these techniques it is presented the premises for the global damper design, for the preload system, for the sensors and for the actuators. The constructed device is composed by three mainly parts: Friction surfaces; normal force control and monitoring; damper base and the friction force monitoring. The damper has two friction surfaces composed by a sphere in contact to a plane. On the preload system two bolts impose an initial DC level for the normal force, this is important to set up the range of normal force necessary for the control law. The normal force control device is composed by a piezoelectric actuator type STACK PPA40L, a piezoresistive load cell and a specific suspension, which is flexible in the direction of the normal force and rigid in the direction tangential to the contact surfaces. Results obtained during the design process are shown as well as the results obtained with initial tests. Based on these results is possible to conclude that the damper will work well to minimize the vibration amplitude in future tests with multi-degree of freedom systems*

Keywords: *Friction damper, semi-active control, hysteresis cycle, test rig design.*

1. INTRODUCTION

Dry friction dampers have been used for the attenuation of vibration in a wide variety of mechanical systems which are not possible to apply viscoelastic materials, fluid based dampers or others viscous dampers. A first example is the application of friction dampers in aircraft engines to reduce the blades vibration amplitudes (Arrao and Nourse 1990). Seismic isolation based on friction was proven be a very useful solution for large civil structures (Lu et al. 2008). In most cases, friction dampers had been studied in a passive way, however, a significant improvement can be achieved by controlling the normal force in the dampers (Dupont et al. 1997). Friction dampers with variable normal force are classified as semi-active devices and their appeal is to have performance levels rivaling the active devices with low level of energy consumption (Dupont et al. 1997).

A brief bibliography review should reveal numerous strategies for control laws in friction damping. Inaudi (1997) proposes that the normal force should be proportional to the absolute value of the prior local peak of damper deformation, the author called damper deformation the relative displacement between the degrees of freedom where has been installed the damper. The best proportion for the normal force has been described by Menq et al. (1986) and by Menq et al. (1986).

Ozbulut et al. (2011) proposed the use of fuzzy logic to actualize the normal force in semi active friction dampers used for huge civil structures. The authors conclude that a passive friction damper can be optimized only for specific excitation forces characteristics, therefore active dampers produces good results for a wide spectrum of excitation forces characteristics.

He et al. (2003) designed a modification for the Inaudi control strategy. This modification actualizes the normal force continuously with the damper deformation. The authors proposed two parameters to adjust their control strategy: Control gain and a boundary layer parameter which means how fast the controller changes the normal force. The aforementioned control strategy demand high levels of control gain, as shown the results obtained by the authors.

ISSN 2176-5480

Nitzsche et al. (2005) propose a control strategy for system where the friction damper has two states only: "ON" and "OFF". In their strategy, the damper accumulates potential energy, by means of the tangential elastic deformation. However, the damper accumulates energy only when the system goes far from its static equilibrium position, this energy never is restored to the system since the damper is turned off when it moves in direction of its static equilibrium position.

Santos, Lepore et al. (2012; 2013) studied different control strategies for friction dampers based on the hysteresis cycle. In these papers three main strategies had been studied with focus on the energy removal by cycle of oscillation, amplitude of the friction force and the control effort. In these papers the receptance curves for a one degree of freedom and the response for a step function coupled to the friction damper are used to evaluate the control strategies performances.

Some of these techniques to maximize the energy dissipation are presented in this paper, i.e., using numerical simulations these are compared and briefly discussed. Based on these control techniques it is presented the premises for the global damper design, for the preload system, for the sensors and for the actuators. The constructed device is composed by three mainly parts: Friction surfaces; normal force control and monitoring; damper base and the friction force monitoring. The damper has two friction surfaces composed by a sphere in contact to a plane. On the preload system two bolts impose an initial DC level for the normal force, this is important to set up the range of normal force necessary for the control law. The control device is composed by a piezoelectric actuator type STACK PPA40L, a piezoresistive load cell and a specific suspension, which is flexible in the direction of the normal force and rigid in the direction tangential to the contact surfaces. The range of the normal force is limited by the preload and by the stiffness of the preload apparatus, consequently by the maximum displacement of the piezoelectric stack. The base for the damper is almost rigid and connected to the damper by means of load cells that measure the friction force. Results obtained during the design process are shown as well as the results obtained with initial tests.

2. NUMERICAL STUDIES OF FRICTION DAMPING

The energy dissipation characteristics of a damper can be understood by its hysteresis loop. The hysteresis loop of a variable friction damper depends greatly on the control algorithm applied. In other words, the same variable friction damper with the same excitation may have different hysteretic behaviors when different control algorithms are applied.

In this work had been used the model to simulate the friction inside the damper as represented in the "Fig. 1".

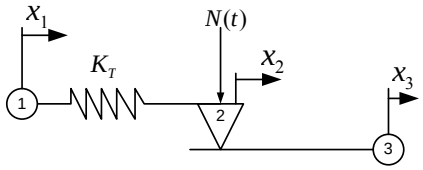

Figure 1. Friction Damping Model

For the proposed model the force between NODE 1 and NODE 3 is written as follow:

$$F_{13} = \begin{cases} K_T(x_3 - x_1) & if \quad |K_T(x_3 - x_1)| < \mu N \\ sign(x_3 - x_1)\mu N & if \quad |K_T(x_3 - x_1)| \geq \mu N \end{cases} \tag{1}$$

Assuming an harmonic motion for $x_1(t)$ and $x_3(t) = 0 \; \forall \; t$ on "Eq. (1)", the normalized hysteresis cycles for the three studied cases are presented in the "Fig. 2".

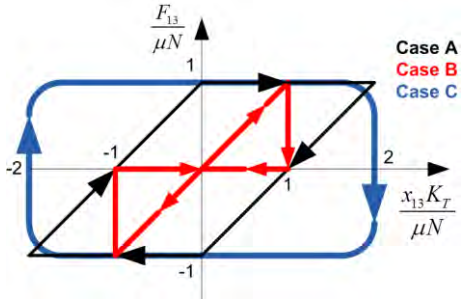

Figure 2. Normalized hysteresis cycles.

An one degree of freedom (DOF) vibratory system, as presented in the "Fig. 3", was used for simulations. Had been adjusted the following parameters: mass $M = 3\ kg$; suspension stiffness $K = 52\ kN/m$; $C = 10\ N/(m/s)$ for viscous damper, which means a damping factor of $\xi = 1.25\%$ and a natural frequency $\omega_n = 20.96\ Hz$. Tangential stiffness for the friction damper has been settled at $K_T = 260\ kN/m$ and friction coefficient was adjusted for $\mu = 0.3$ in order to calculate and simulate all studied control cases. These values represent the parameters expected for the designed and

ISSN 2176-5480

constructed test rig. These values were taken during the design of the test rig and had been used only for the initial simulations.

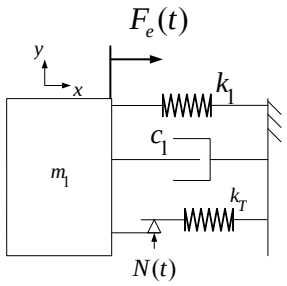

Figure 3. One degree of freedom vibratory system.

To confirm the implemented algorithm for numeric integration, the following receptance curves had been calculated. It should be noted the transition from free system to the completely stuck configuration (black line) as the relation $F_e(t)/N(t)$ decreases.

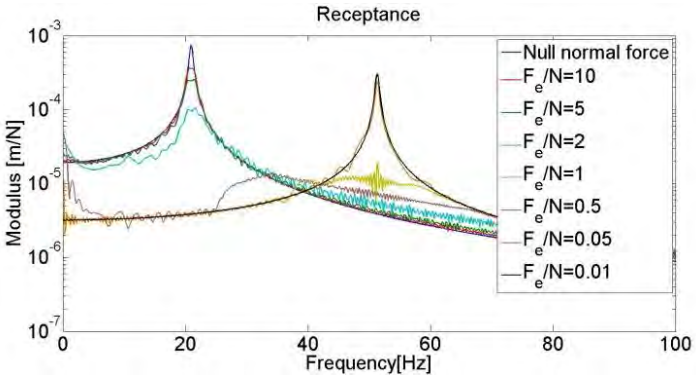

Figure 4. Receptance curves for different relations between excitation force ($\boldsymbol{F_e}$) and normal force $\boldsymbol{N}$.

From "Fig. 4" is possible to verify that the proposed numerical integration algorithm presents almost the same behavior of harmonic balance method (HBM). The HBM could not be used here due the complexity to implement the control strategies. The mainly difference between them comes from the presence of multi-harmonics in the solution and due this the curve appears more roughly than HBM results. It is possible also to determine that the limit for a passive damper stray between the interval: $0.05 \leq \frac{F_e}{N} \leq 0.5$. Outside this limit, or the Coulomb friction forces is too low to dissipate the energy, or the damper stay the major part of time at stuck condition.

The control laws to reproduce the hysteresis cycles were numerical implemented as described at the following sub-sections.

2.1 Control law for hysteresis cycle namelly "CASE A"

To reproduce this hysteresis cycle the normal force varies with the following law:

$$N_1(t) = G|P[\Delta(t)]| \tag{2}$$

Where $P[\Delta(t)]$ is the last peak or valley in the damper deformation $\Delta(t) = (x_3 - x_1)$ as stated in "Eq. (1)". Should be noticed that this formulation has been proposed originally by Inaudi (1997). However, the difference between the original formulation and what is used in this work stay in the control gain G, i.e., the gain is sttled for maximize the energy dissipation in $G = K_T/2\mu$. The necessity to use the last peak is clear present when the system is excited with a non-periodic force, since for a periodic force the operator $P[\Delta(t)]$ leads to a constant value.

ISSN 2176-5480

2.2 Control law for hysteresis cycle namelly "CASE B"

To reproduce the idea for the maximum energy removal strategy proposed by Nitzche (2005) has been implemented the following law:

$$N_2(t) = \begin{cases} G|P[\Delta(t)] \; if \; sign\left(\frac{d\Delta(t)}{dt} * \Delta(t)\right) \geq 0 \\ 0 \qquad\qquad if \; sign\left(\frac{d\Delta(t)}{dt} * \Delta(t)\right) < 0 \end{cases} \tag{3}$$

The control gain G and the operator $P[\Delta(t)]$ hold the same properties as stated for "CASE A".

2.3 Control law for hysteresis cycle namelly "CASE C"

Originally, the law that reproduces the hysteresis cycle as presented in "Fig. 2" has been described by He et al (2003) based on Inaudi formulation. In this work it is used a modification proposed by Santos and Lepore (2013) on the formulation proposed by Yang et al. The originally equation is:

$$N_3(t) = \beta(G|P[\Delta(t)]|)\left|\tanh\left[\alpha\frac{d\Delta(t)}{dt}\right]\right| \tag{4}$$

Where β is the control gain and α is the boundary layer parameter, both as proposed by Yang et al (2003). To reduce the control gain β was introduce the terms $G|P[\Delta(t)]|$ which are the control strategy for the "Case A".

The control law defined in "Eq.(4)" is strongly dependent of the deformation velocity $d\Delta(t)/dt$ to setup the normal force as fast as possible. However, as written the normal force is always settled using the deformation velocity from the last time step, so in order to improve the algorithm performance the originally equation is changed as written below:

$$N_4(t) = \beta(G|P[\Delta(t)]|)|\tanh[\alpha V(t)]| \tag{5}$$

where:

$$V(t) = \frac{d\Delta(t)}{dt} + \frac{d^2\Delta(t)}{dt^2} * dt \tag{6}$$

This modification anticipates the control effort adjusting the normal force of the system in the next step based on the estimation of the future state variables not in the state variables for the actual time step.

3. NUMERICAL RESULTS

All results were obtained using an 1 DOF vibratory system described in the last section. It is important to notice that this system is similar to the test rig constructed in the laboratory. First results had been obtained using an harmonic excitation with $5\,N$ of amplitude and $100\,Hz$ of amplitude. From the system response it is possible to plot the normalized hysteresis cycles as in "Fig. 5".

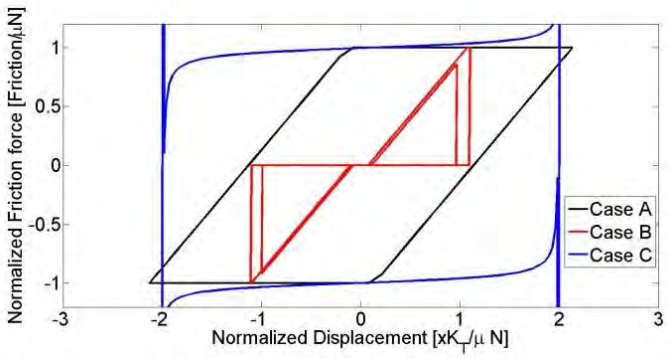

Figure 5. Numerically simulated hysteresis cycles

It is possible to assume that the approximations for all cases of hysteresis cycles as idealized before, even with the differences at the extremes for the "Case C", are suitable for the simulations. The spikes in the hysteresis cycles for "Case C" can be assigned to the high value of adopted for α, since small values of α do not produce the spikes but the

ISSN 2176-5480

hysteresis would appear as an ellipse.

To analyze the performance of the control strategies had been used a sine sweep excitation force with amplitude settled in $F_e = 5\ N$ and initial normal force in $N = 10\ N$. These values had been choose to compare the results for controlled friction damper and the passive damper results as shown in "Fig. 4" for $F_e/N = 0.5$.

Analyzing the results in "Fig. 6" is possible to affirm that the all controlled systems produce responses better than the responses for the linear systems, i.e., the 1 DOF system with uncoupled K_T $(N(t) = 0)$ and the completely stuck damper. The responses for these linear systems are represented by the blue and black lines respectively. These systems present natural frequencies at $\omega_n = \sqrt{k_1/m_1}$ and $\omega_n = \sqrt{(k_1 + k_T)/m1}$.

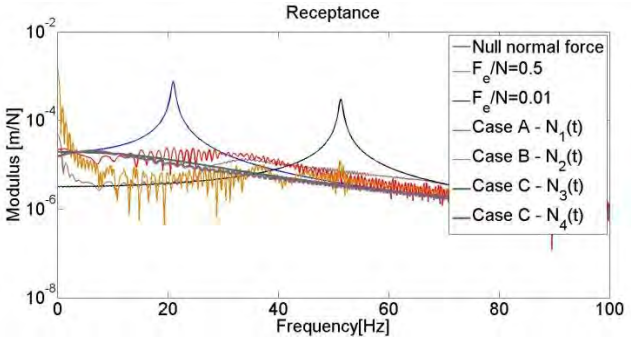

Figure 6. Receptance curves for controlled dampers.

The systems controlled with strategies for "Case A" and "Case B" had similar performances. Their receptance curves present almost the same amplitude over the studied frequency spectrum of the passive case with $F_e/N = 0.5$. The receptance curves for these cases present also some noise, that comes from the frequently transients introduced by the abruptly changes in the normal force, this characteristic is more clearly for case B, which hysteresis cycle has more discontinuities.

Both control strategies used to reproduce the hysteresis cycles for "Case C" provide very similar receptance curves reducing the dynamic response also in lower frequencies, a region in the spectrum where the others two control strategies fails. Should be observed in the "Fig. 6", the absence of resonance peaks or spikes, the lasts caused by abruptly changes in the friction force presents in "Case A" and "Case B".

The proposed laws for "Case C", equations (4) and (5), reduce the demand for large control gains as the original work proposed by Yang et al (2003), the authors had been used gains not lower than 100,000 times. To obtain the presented results had been used the parameters as shown in "Tab. 1".

Table 1. Control parameters

	$\boldsymbol{\alpha}$	$\boldsymbol{\beta}$
"Eq. (4)" - $\boldsymbol{N_3(t)}$	10	10
"Eq. (5)"- $\boldsymbol{N_4(t)}$	1	0.5

Yang et al (2003) had been mentioned that small α leads to a more smooth controllers and consequently to a more efficient auto adaptive control law. In this sense should be noticed that the controller obtained from "Eq. (5)" is more efficient.

Other difference between the two controllers, $N_3(t)$ and $N_4(t)$, is the amplitude of the friction force that has been used to damper the system. It is possible to observe, in the "Fig. 7", that the controller $N_4(t)$, demands a friction force lower than $N_3(t)$ after 2.5 seconds, or when the sweep sine passed by 60 Hz. In this sense and that small friction generally conducts to lower wear rates the controller $N_4(t)$ can leads to a longer life of friction devices.

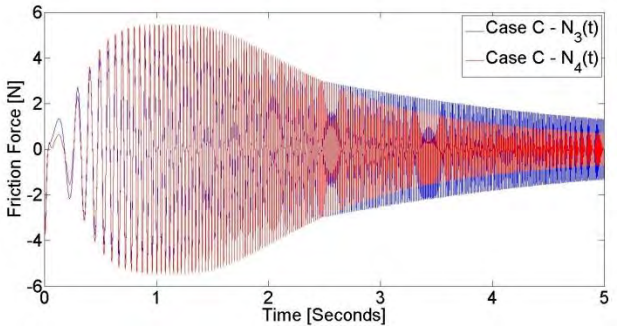

Figure 7. Friction force for sine sweep excitation.

ISSN 2176-5480

A drawback of the passive friction dampers is that they can change the static equilibrium position of the vibratory system, sometimes this characteristic forbid the application of friction dampers. To analyze this behavior all controlled dampers had been submitted to a step excitation force as follow:

$$F_e(t) = \begin{cases} 5\ N\ if\ 2 \leq t \leq 4 \\ 0\ N \quad otherwise \end{cases} \tag{7}$$

It is possible to observe in "Fig. 8" that constant normal force (passive damper) and the controlled damper for "Case A" fail in the sense that they change the static equilibrium position. Analyzing the performance for the other controllers it is possible to see that the controller $N_3(t)$ had been produced the lower overshoot. The controller $N_4(t)$ had a similar performance from $N_3(t)$. In terms of settling time the controllers $N_3(t)$ and $N_4(t)$ had almost the same performance even in the presence of different values for the parameter α.

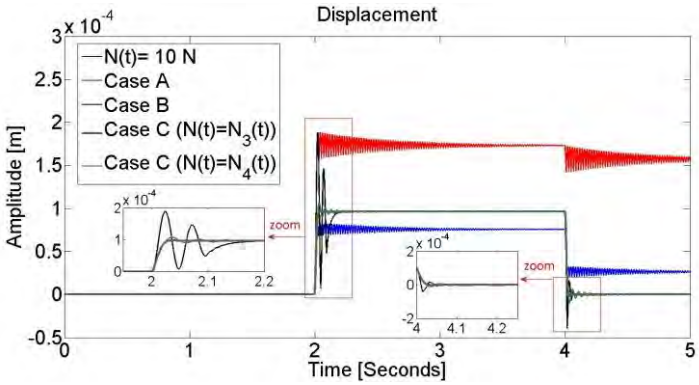

Figure 8. Step responses

Neither of the two controllers used to reproduce the hysteresis cycle of "Case C" changed the static equilibrium position, so they can be considered suitable for occasions where the static equilibrium position cannot be changed.

4. TEST RIG DESIGN

Based on the variables analyzed during the numerical simulations performed in the last session had been defined the following parameters to be measured during the experimental tests:

a) Degree of freedom displacement;
b) Relative displacement between the damper anchorage points;
c) Normal force;
d) Friction force;
e) Excitation force;

Based on these necessities the test rig has been designed in order to uncouple the force measurement in the directions normal and tangential to surfaces in contact. The "Fig. 9" shows the schematic diagram of the friction damper. In this diagram are shown two sphere to plane contacts pairs which compose the friction damper itself.

In the "Fig. 9" is possible to verify the piezoelectric actuator (3), the load cell to measure normal force (4), the damper structure (6) and the contact spheres (2) positioned in an axis oriented normally to the contacts surfaces. As positioned on the damper all displacement of the piezoelectric actuator produces a variation in the normal force, which is measured by the load cell (4). The damper structure had been designed to be very flexible in the direction normal to the surfaces contacts and very rigid in the tangent direction. The damper structure (6) is composed by four beams where had been machined circular slots, i.e., flexure hinges. These flexure hinges work as rotary joints without frictions. (Lobontiu et al. 2002).

As designed the flexures hinges have an elastic constant in the normal direction of $12.42\ N/mm$. Considering the maximum displacement of the piezoelectric actuator, which is $40\ \mu m$, one calculates the maximum force produced by the damper structures equals to $0.49\ N$, therefore much lower than the actuator maximum force $1500\ N$.

ISSN 2176-5480

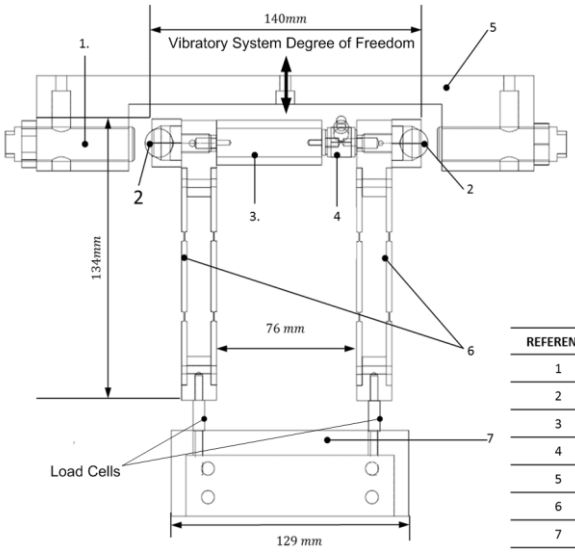

REFERENCE	COMPONENT
1	Preload bolt
2	Contact splere
3	Actuador PPA40L
4	Load Cell
5	Damper moving base
6	Damper structure
7	Inertial frame

Figure 9. Schematic diagram for the friction damper test rig.

The preload bolts (1) had been designed to adjust the mean value of the normal force. Figure 10 shows an example of normal force preload adjustment. In this procedure the actuator had been commanded to stretch $10\ \mu m$, which results in $5\ \mu m$ from the neutral point for the left and right sphere displacement. After the actuator reaches the expanded position the bolts are tight until the load cell register the contact between the spheres and the bolts. From this point the actuator has been commanded to the $0\ \mu m$ position. Sweeping the actuator displacement from 0 up to $40\ \mu m$ the load cell (4) registered the force profile indicated in the "Fig. 10". As can be seen the normal force rest at zero until the actuator displacement reaches $10\ \mu m$, from this point the load increases almost linearly until its maximum value of $130\ N$. The line slope is equal to the global stiffness, which is $8195\ N/mm$ in this case, a value much higher than the damper structure stiffness in the same direction. Therefore, the normal force depends on the actuator displacement and the global stiffness.

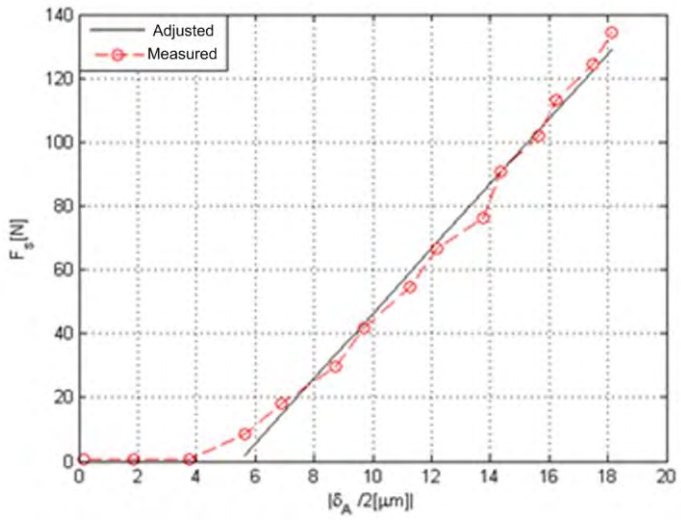

Figure 10. Normal force adjustment procedure.

In the "Fig. 11" is shown the physical model for the normal force control device. In this model is possible to verify that the ideal condition is when the load cell stiffness tends to infinite and the flexure hinges stiffness tends to zero. Therefore, in ideal condition the length variation ΔL will lead to the maximum strain in the contact bodies giving the maximum amplitude in the normal force control. However, as a perfectly rigid load cell does not work as the strain gage will not be deformed, therefore, no output signal can be generated by the load cell. In this case a finite element model has been used to maximize the stiffness and the sensibility together.

ISSN 2176-5480

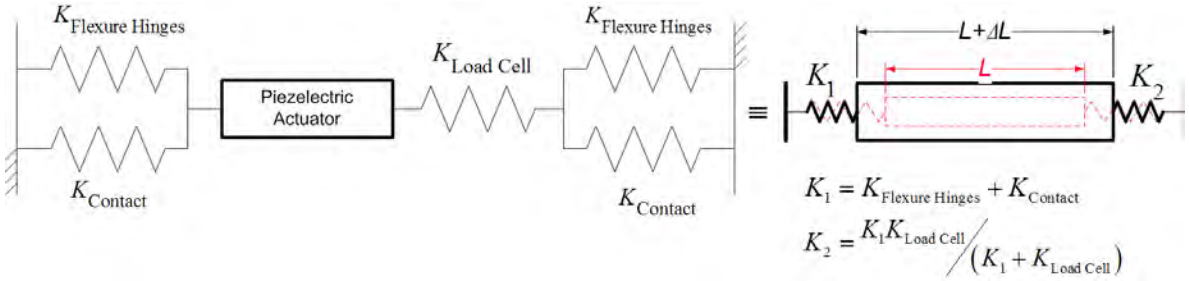

Figure 11. Physical model of the normal force control device.

The load cell used to measure the normal force had been designed specifically for this test rig. This load cell is basically a ring that is deformed under action of a traction or compression load. From a numerical simulation using finite element methodology is possible to observe the strain during the application of the normal force as shown in "Fig. 12". The strain gages had been placed at positions indicated by the color red and blue. Using this finite element model the load cell stiffness has been identified with the value of $42372.9\ N/mm$.

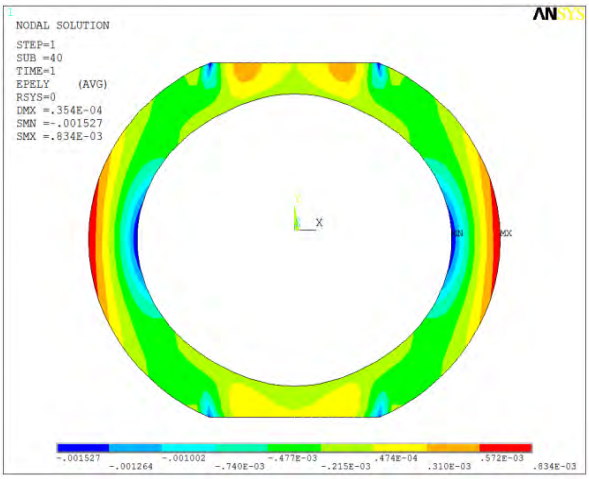

Figure 12. Load cell simulation.

Considering the global stiffness $K_G = 8195\ N/mm$, the Flexure hinges stiffness $K_{Flexure\ Hinges} = 12.42\ N/mm$ and the load cell stiffness $K_{Load\ Cell} = 42372.9\ N/mm$ and the physical model in "Fig. 11" is possible to obtain the following contact stiffness:

$$\frac{F}{\Delta L} = K_{Global} = \frac{K_1}{2+\frac{K_1}{K_{Load\ Cell}}} \rightarrow K_{Contact} \cong 13721\ N/mm \tag{8}$$

To verify the damper performance, it was attached to a one degree of freedom. The vibratory system is composed by a table suspend by four beams, which permit the displacement preferentially in the direction indicated in the "Fig. 13". The vibratory system suspension can be changed to adjust the natural frequency in a desired value. As adjusted in the conducted test the table suspension stiffness is $K_T = 66590\ N/m$, which is associated to a mass of $m = 4.217\ Kg$ to result in a natural frequency of $20\ Hz$. The instrumentation used was:

a) Accelerometer to measure the DOF acceleration;
b) Load cell to measure the excitation force when it is necessary;

ISSN 2176-5480

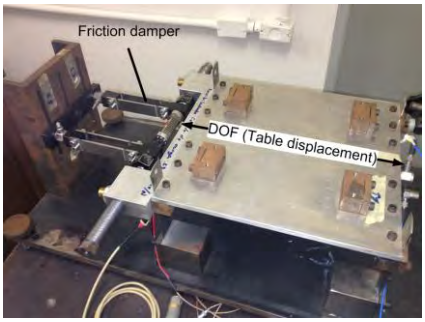

Figure 13. Test rig with the friction damper coupled to a one degree of freedom (DOF) vibratory system.

First test was conducted putting a non-null displacement as initial condition, after that, the system was leave to vibrate under influence of the friction damper. The normal force has been adjusted in $105\ N$ and the friction coefficient for the materials in contact is 0.20. These results are shown in "Fig. 14".

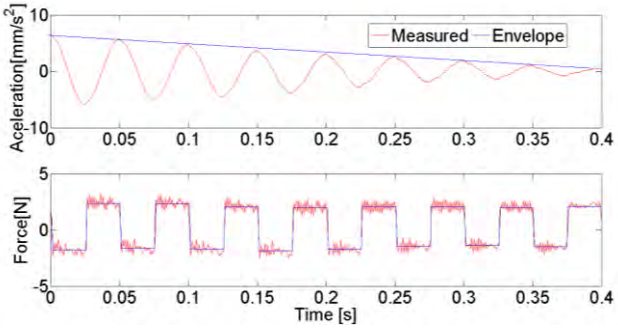

Figure 14. Free response for the vibratory system under influence of the friction damper.

Should be evidenced the measured friction force, red line in "Fig. 14". This force has the behavior as stated by the Coulomb law. The oscillation present in the measured force can be attributed to the vibration of the frame assumed as an inertial frame. To remove this oscillation the frame should be stiffened.

The envelope for the pikes in the displacement has been used to calculate the friction force resulting in a value of $1.85\ N$. The envelope for the measured friction force has the limit for static friction of $2.3\ N$. This difference can be attributed the flexibility off the damper support and the hypothesis of pure Coulomb friction.

To quantify the deviation from the friction model shown in "Fig. 1" and represented by the macro slip numerical model in "Eq. (1)" has been conducted a test with a harmonic excitation force of $20N@10\ Hz$. The hysteresis cycle has been plotted and the model from "Eq. (1)" has been adjusted as in "Fig. 15", from this curve fitting procedure the estimated tangential stiffness is $1121.5\ N/mm$. Some deviations are observed an can be assigned to the flexibility of the frame assumed as an inertial one, some surface roughness and misalignment between the bolt surface and the direction of the vibratory system DOF. However, the adjusted curve is very similar to the experimental one, which permits conclude that the test rig works as expected in its design.

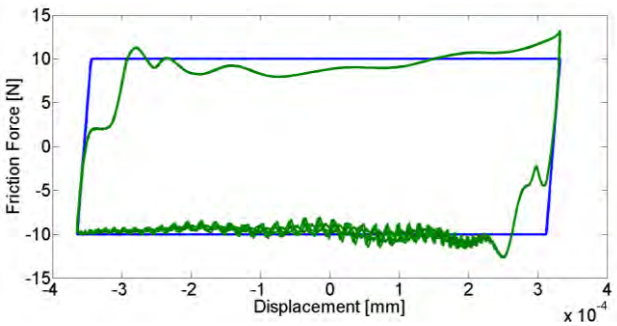

Figure 15. Measured and estimated hysteresis cycle.

First results show that the test rig is suitable to confirm numerical simulations.

ISSN 2176-5480

5. CONCLUSION AND FUTURE WORKS

Had been presented numerical simulations for friction dampers with variable normal force. Control law for Case A reduces the resonance peak almost 100 times. Although the resonance peak reduction, this control law has a poor performance at low frequencies. Case B and Case A had a similar performance. Only Case A control law fails changing the static equilibrium position for step response. Both controls laws used for case C have similar performance and produce the greater reductions in the resonance peaks. The controller $N_4(t)$ achieves almost the same results of the controller$N_3\ (t)$, however with lower values for parameters α and β, so that, the controller $N_4\ (t)$ can be considered more adaptive than controller N_3 (t). Both controllers are suitable for cases where the static equilibrium position cannot be changed and produce a very good step response.

Based on these simulations the test rig has been designed to measure the force and displacements that are necessary to characterize the friction damper. Had been designed a support for the damper which permits the application of the normal force independently of the friction force level. The preload system can be used to set the mean level for the normal force. The actuator displacement associated to the contact stiffness and the bolt stiffness limit the amplitude of variation for the normal force. The usage of two load cells, to measure the friction force, give some stability to the damper support without loses in the precision of the measured force.

Future works will be conducted using the presented control strategies. Since is possible expand the number of the degrees of freedom in the vibratory system, are planned experiments with 3 degrees of freedom in order to explore the influence of the damper position.

6. REFERENCES

Arrao, A. S. and J. G. Nourse (1990). Vibration Damping in Rotor Blades. UK Patent Application. UK, General Electric Company: 17.

Dupont, P., P. Kasturi, et al. (1997). "SEMI-ACTIVE CONTROL OF FRICTION DAMPERS." Journal of Sound and Vibration 202(2): 203-218.

He, W., A. Agrawal, et al. (2003). "Novel Semiactive Friction Controller for Linear Structures against Earthquakes." Journal of Structural Engineering 129(7): 941-950.

Inaudi, J. A. (1997). "MODULATED HOMOGENEOUS FRICTION: A SEMI-ACTIVE DAMPING STRATEGY." Earthquake Engineering & Structural Dynamics 26(3): 361-376.

Lobontiu, N., J. S. N. Paine, et al. (2002). "Design of symmetric conic-section flexure hinges based on closed-form compliance equations." Mechanism and Machine Theory 37(5): 477-498.

Lu, L.-Y., G.-L. Lin, et al. (2008). "Stiffness controllable isolation system for near-fault seismic isolation." Engineering Structures 30(3): 747-765.

Menq, C. H., J. Bielak, et al. (1986). "The influence of microslip on vibratory response, part I: A new microslip model." Journal of Sound and Vibration 107(2): 279-293.

Menq, C. H., J. H. Griffin, et al. (1986). "The influence of microslip on vibratory response, Part II: A comparison with experimental results." Journal of Sound and Vibration 107(2): 295-307.

Nitzsche, F., T. Harold, et al. (2005). "Development of a Maximum Energy Extraction Control for the Smart Spring." Journal of Intelligent Material Systems and Structures 16(11-12): 1057-1066.

Ozbulut, O. E., M. Bitaraf, et al. (2011). "Adaptive control of base-isolated structures against near-field earthquakes using variable friction dampers." Engineering Structures 33(12): 3143-3154.

Santos, M. B. d. and F. P. Lepore (2013). Assessment on Control Strategies of Friction Dampers. Word Tribology Congress 2013. Turim, Italy, Associazione Italiana di Tribologia.

Santos, M. B. d., F. P. Lepore, et al. (2012). Numerical Assessment of Smart Spring to Attenuate Structural Vibrations. XVIII Symposium on Vibrations, Chocs & Noise. Paris, France.

7. ACKNOWLEDGEMENTS

The authors grants for the financial support from CNPq, Capes, Fapemig and from POSMEC/UFU.

8. RESPONSIBILITY NOTICE

The authors are the only responsible for the printed material included in this paper.